Ceramics International 49 (2023) 25516–25529

Contents lists available at ScienceDirect

Ceramics International

journal homepage: www.elsevier.com/locate/ceramint

Effect of trimethylamine borane (TMAB) bath concentration on electrodeposited Ni–B/TiC nanocomposite coatings

Ersin Ünal [a], Abdulkadir Yaşar [b,*], İsmail Hakkı Karahan [c]

[a] Department of Mechanical Engineering, Engineering Faculty, Osmaniye Korkut Ata University, 80000, Osmaniye, Turkey
[b] Department of Mechanical Engineering, Ceyhan Engineering Faculty, Çukurova University, 01190, Adana, Turkey
[c] Department of Physics, Faculty of Arts and Sciences, Mustafa Kemal University, 31040, Hatay, Turkey

ARTICLE INFO

Handling Editor: Dr P. Vincenzini

Keywords:
Ni-B/TiC
Electrodeposition
Composite coatings
Ni–B alloy
TMAB
Microhardness
Corrosion

ABSTRACT

In this study, stainless steel material was coated with Ni–B alloy-based, TiC particle reinforced composite film using electrochemical deposition method. The properties of the obtained Ni–B/TiC nanocomposite coatings were investigated in terms of the effect of trimethylamine borane (TMAB) bath concentration, which is a boron source. In addition, the data of pure Ni, Ni–B alloy and stainless steel are presented together for comparison. According to the cyclic voltammogram (CV) analysis, it is seen that TMAB contributes to increasing the deposition rate. In the crystal structure analysis, the effect of TMAB was weaker at low TiC bath concentrations, while the effect of TMAB was more dominant at high TiC bath contents. The crystal grain size values of nanocomposite coatings vary between 5.8 and 16.8 nm, and these values decrease up to 86% when compared to the crystal grain size of the pure Ni coating. Although the increase in TMAB initially causes an increase in the microhardness of nanocomposite coatings, when the TMAB value was further increased, it was observed that the microhardness decreased even more compared to the previous initial value. The highest hardness value was obtained in the sample produced at 5 g/l TiC and 6 g/l TMAB bath contents, and this value was 817 HV. Compared to this value, it was observed that the hardness of pure Ni was 65% lower. It was observed that TMAB did not have significant effect on the coating morphology, but the increase in TMAB caused an increase B content and a decrease in the TiC content in the nanocomposite coating. Furthermore, it was revealed that the increase in TMAB bath concentration caused an improvement on corrosion resistance. The corrosion current of the composite sample with 9 g/l TMAB concentration, which showed the best corrosion performance, decreased by 85% compared to pure nickel.

1. Introduction

Nickel-based coatings are widely used as protective coatings on an industrial scale to protect various types of parts against external influences such as corrosion and wear. Although pure nickel shows good corrosion resistance, wear performance is insufficient due to low strength and hardness. Alloying of nickel significantly increases its hardness, wear and corrosion resistance. The increase in hardness of nickel alloy coatings depends on the type of alloying elements and the structural changes affected by their co-deposition, and grain size reduction alongside solid solution hardening are the main hardness increasing mechanisms [1–3]. In recent years, the importance of Ni–B alloy coatings has been increasing for industries that require high corrosion, mechanical and tribological resistance such as automotive, aerospace and chemistry [4]. Ni–B alloy coatings have high hardness, good wear and corrosion resistance, and good solderability [5,6]. It is also known that Ni–B alloy coatings have good electrical, antibacterial, electromagnetic and lubricity properties that increase their applications in many sectors such as nuclear, petrochemical, electronics [7]. The electrochemical deposition technique for Ni–B alloys offers several advantages such as high growth rate, low bath temperature, good stability, easy control of production parameters and uniform distribution of boron element in the coating [4,8]. However, further improvement of properties is required to extend service life in extreme environments. For this purpose, many studies have focused on optimizing the manufacturing process, alloying with other elements, or adding a second reinforcement phase to the Ni–B matrix [9]. The variety and increasing availability of nanoparticles and low temperature and cost-effective production are

* Corresponding author.
E-mail address: ayasar@cu.edu.tr (A. Yaşar).

https://doi.org/10.1016/j.ceramint.2023.05.092
Received 18 January 2023; Received in revised form 3 May 2023; Accepted 9 May 2023
Available online 10 May 2023
0272-8842/© 2023 Elsevier Ltd and Techna Group S.r.l. All rights reserved.

constantly increasing the interest in composite electroplating. The most important aspects in the production of these materials are the high deposition rates and homogeneous distribution of the particles in the metallic matrix. Among the methods used to deposit nanostructured composites, electrodeposition technique can achieve a smoother surface, higher microhardness, and a better interface between the particle and the metal matrix [10–12]. In the literature review, it is seen that Ni based coatings are successfully strengthened by reinforcement with various ceramic particles. It is possible to give particles such as WC [13], B_4C [14,15], YSZ [7], hBN [4,16,17], SiC [18], SWCNT [19], TiN [20], AlN [21], graphene [22–25] as an example to the current studies.

Titanium carbide is one of the important carbides formed as a result of the reaction of the element titanium, which is in the 4th group of the periodic table, with carbon. It is a reinforcing nano powder mostly used in structural applications where safety is the main factor, aerospace, automobile industries and special cutting tools. TiC has a cubic crystal structure and a black color. This ceramic material has a density of 4.93 g/cm^3 as well as a very high melting point of 3200 °C. Since TiC has excellent properties such as high hardness, high melting temperature, low density, high wear resistance, high mechanical hardness and chemical stability, it can be considered as one of the effective reinforcements for Ni-based coatings [12,26]. In recent years, it has been seen that TiC is preferred as reinforcement particles in composite coatings to increase wear and corrosion resistance to be used in different applications [27,28] obtained nanocomposite coatings with Ni–W alloy main structure and TiC particles reinforcement by pulsed electrodeposition method on mild steel substrate. According to the authors, the highest hardness value was obtained at 15 g/l TiC bath concentration. They also reported that TiC reinforcement provides an improvement in corrosion resistance and this situation is caused by the barrier effect of the particles. Karbasi et al. [12] reinforced the nickel matrix with TiC particles and deposited nano-composite coating on the brass substrate with direct current in a Watts type nickel bath. According to the authors, at the current density of 70 mA/cm^2, which is the optimum value, the nickel nucleation rate increased, and as a result, grain growth was limited, and they stated that the best composite morphology was formed. Li and Zhang [29] performed ultrasonic assisted deposition and used copper substrate in their work in which they strengthened the Ni–B alloy with TiC particles. They investigated the effects of current density and deposition time and reported that there was a significant improvement in corrosion resistance with the contribution of ultrasonic assisted deposition with reinforcement. Fayyaz et al. [30] analyzed the effect of particle bath concentrations on structural, mechanical and corrosion properties of composite coatings with Ni–P alloy main structure and TiC reinforcement. The authors reported that the hardness and corrosion resistance increased with the increase of TiC particle concentration in the bath, but after a certain value, the hardness decreased.

In this study, Ni–B alloy was reinforced with nano TiC particles and coated on a stainless steel (AISI 304) substrate by electrochemical deposition method. It is seen that only one study has been carried out about these coatings in the literature [29]. Alloying with boron seriously affects the properties of Ni–B/TiC nanocomposite coatings, and in this study, the TMAB bath concentration effect was investigated for the first time in the literature for Ni–B/TiC nanocomposite coatings. AISI 304 quality stainless steel preferred as the substrate material, is the most widely used material in this class in the world. It is used in many applications due to its economic properties, mechanical properties, corrosion resistance and weldability [31]. Although there are other options that can be used as a boron source apart from TMAB in order to alloy nickel with boron in the electro or non-electric plating method, as seen TMAB is generally preferred in the literature. Also, Sheu et al. [32] stated in their studies on Ni–B that DMAB, which can be used as a boron source in electrochemical deposition, dissolves at higher temperatures (>75 °C) than TMAB, and the plating bath with TMAB is more stable than the other. In the light of this information, it can be stated that TMAB is a more suitable boron source for Ni–B alloy deposition. In studies on Ni–B alloy-based electrodeposited composite coatings, it is seen that the bath concentration effect of boron source (TMAB or dimethylamine borane (DMAB) and others) has not been studied much. Moreover, in studies examining the TMAB effect, there was not much detailed analysis, but in this study, the TMAB effect was discussed in such detail for the first time. It is thought that this study will make up for the deficiency in this regard to some extent. According to the results, it has been observed that the mechanical and corrosion properties of the produced nanocomposite coatings have been significantly improved, and it has been understood that it is a suitable alternative for machine parts especially in harsh operating conditions.

2. Experimental procedure

In this experimental study, composite coatings with TiC particle reinforced Ni–B alloy main structure (size smaller than 500 nm) were coated on a stainless steel (AISI 304) substrate by conventional electrodeposition method. Electrodeposition of the coatings was carried out with the CH Insturment electrochemical analyzer. The coatings are produced on the basis of Watts type nickel bath and the necessary additives were added to obtain the nanocomposite coating. Production parameters and electrolyte content used in coating production are given in Table 1. A traditional Watts type nickel bath is used for the electrodeposition of nickel-based materials. It was described by Oliver Watts in 1916. Nickel sulfate ($NiSO_4.6H_2O$) is the main source of nickel in a Watts bath. Nickel sulfate is of high purity and low in cost. In addition, it is preferred in practice because it has little abrasive effect on the equipment used. Another source of nickel in a Watts-type nickel bath is nickel chloride ($NiCl_2.6H_2O$). Nickel chloride chemical is also low in cost and has a high purity, but it has higher corrosive properties than nickel chloride. Therefore, the amount of nickel chloride in the bath is much less than nickel sulfate. Furthermore, nickel sulfate compound causes less internal stress in the coating than nickel chloride [33,34]. In addition, trimethylamine borane complex (TMAB), one of the materials used for alloying with boron, was added to the electrolyte in various amounts. A three electrode electrodeposition system was used in the production of the coatings. A platinum wire rod was used as the anode and a saturated calomel electrode (SCE) was used as the reference electrode. The stainless steel material used as the cathode (substrate) was adjusted to have an area of 4 cm^2 and treated a series of processes before the coating operation. In order to clean the surface to be coated from various dirt, rust and oil layers, it was sanded with sandpaper from coarse to fine and then cleaned with acetone and rinsed with pure water. Then, the substrate was etched in hydrochloric acid (HCl) for 1–2 min and it was rinsed with distilled water and made ready for the coating process. After

Table 1
Bath parameters and electrolyte content [44].

Bath parameters		Value
Current density		50 mA/cm^2
pH		4
Temperature		43 ± 1 °C
Time		60 min
Bath mixing speed		200–300 rpm
Ultrasonic mixing before deposition		30 min
Electrolyte content	**Mission**	**Amount**
$NiSO_4.6H_2O$ (Nickel sulfate hexa hydrate) % 99.99	Nickel source	240 g/l
$NiCl_2$. $6H_2O$ (Nickel chloride hexa hydrate) % 98	Nickel source	45 g/l
H_3BO_3 (Boric acid) % 99.5	Complexing agent	30 g/l
Trimethylamine borane complex (TMAB) % 97	Boron source	3–9 g/l
Titanium Carbide powder (TiC) % 99 nano size	Reinforcement particle	3–12 g/l
Sodium dodecyl sulfate (SDS) % 99	Surfactant	0.5 g/l
Saccharin % 98	Grain reducer	2 g/l

coating, the material was rinsed with distilled water and left to dry at room temperature. The electrolyte, which is the other stage of the coating, was prepared from the necessary chemicals and additional materials in certain proportions and was subjected to ultrasonic agitation for 30 min so as to disperse the possible agglomeration of TiC particles before deposition. Hielscher UP 200S brand and model device was used for ultrasonic mixing setting the cycle value to be 1 and the amplitude value to be 70% (~20 kHz). In addition, another important issue, which is the sinking of the particles in the bath and coming to the surface, was prevented by adding the surfactant sodium dodecyl sulfate (SDS) to the electrolyte. The substrate surface to be coated was positioned vertically in the electrolyte and a distance of about 3 cm was left between the substrate (cathode) and the anode. The bath temperature was kept at 43 ± 1 °C during deposition. The deposition bath pH was adjusted to 4. The storage time was limited to 60 min and the baths of the nanocomposite coatings were mixed with a magnetic stirrer during deposition. In addition, saccharin was added to the deposition bath at certain rates to reduce the internal stress of the nanocomposite coatings and to refine the grain structure. The color of the bath ready before deposition turns into a completely black appearance due to TiC particles. The bath was freshly prepared again for each sample deposition. In the electrochemical deposition process, the bath is open to the ambient air. In our cyclic voltammetry (CV) experiments, CH Insturment electrochemical analyzer was used and the scanning speed was determined as 10 mV/s. In the CV graph, it was seen that the deposition on the cathodic side starts around −0.7 V, the dissolution on the anodic side starts around −0.4 V and ends around 0.4 V. Considering these matters, the potential range scanned in our CV experiments was chosen between −1.2 V and 1.2 V. Electrodeposition assembly and electroco-deposition process schema are given in Fig. 1.

The XRD patterns of the samples were obtained to characterize the crystal structures. PANalytical brand Empyrean model XRD device, which produces CuKα radiation in the range of 2θ = 20°–100°, at 40 kV and 30 mA values, was used (λ = 1.5418 Å) to obtain X-ray diffraction patterns. The formulas given below were used in calculation of the average crystal grain size (D) and microstrain (ε) values of the samples [35–41].

$$D = \frac{0.94\,\lambda}{\beta\,cos\,\theta} \tag{1}$$

In the Debye-Scherrer equation (1), λ is the X-ray wavelength, β is the value in radians of the half-maximum width of the relevant peak (FWHM), θ is the Bragg reflection angle of the relevant peak [38,39,41].

$$\varepsilon = \frac{\beta}{4\,tan\,\theta} \tag{2}$$

Equation (2) is used in the calculation of microstrain [35,39].

The following formula was used calculating the relative texture coefficient $RTC_{(hkl)}$ values [16,42].

$$RTC_{(hkl)} = 100 \times \frac{TC_{(hkl)}}{\sum TC_{(hkl)}} \tag{3}$$

In this formula (3), where $TC_{(hkl)}$ is the texture coefficient of (hkl) plane, and $\sum TC_{(hkl)}$ is the sum of the texture coefficients of all planes in the XRD pattern. The texture coefficient was calculated with the following equation [16,43].

$$TC_{(hkl)} = \frac{I_{(hkl)}}{\sum I_{(hkl)}} \times \frac{\sum I_{0(hkl)}}{I_{0(hkl)}} \tag{4}$$

In this equation (4), where $I_{(hkl)}$ is the intensity of the peak corresponding to (hkl) plane, and $\sum I_{(hkl)}$ is the sum of the intensities of all the peaks in the pattern. $I_{0(hkl)}$ and $\sum I_{0(hkl)}$ values are the intensity of the relevant peak and the sum of the intensities of all the peaks in the pattern, respectively, obtained from the reference card. In RTC calculations, XRD pattern data with ICDD reference code 96-210-2276 of nickel were used.

FEI brand Quanta 650 Field Emission model device was used to obtain surface and section morphologies and chemical content analysis. In the measurement of microhardness values, 500 g load was applied on the sample for 10 s. Measurements were taken from at least 10 different regions in each sample and the average of these measurements was accepted as the microhardness value. As a result of the microhardness measurements, the hardness values that deviated excessively from the average were not included in the general average of the sample. Microhardness measurements were conducted with with the Future-TECH FM-700e brand and model device.

Corrosion performances of electrochemically deposited Ni–B/TiC nano composite coatings were analyzed by Tafel extrapolation (potentiodynamic polarization curve) and electrochemical impedance spectroscopy (EIS) methods. CH Insturment electrochemical analyzer was utilized for corrosion analysis. Tafel experiments were carried out in the potential range from 0.25 V below the open circuit potential to 0.25 V above, at a scanning rate of 1 mV/s and in a solution containing 3.5% sodium chloride (NaCl). The samples were kept in a solution containing 3.5% NaCl for 1 h to obtain a balanced potential value before performing the Tafel measurement. Electrochemical impedance spectroscopy studies were carried out with an AC current of 10 mV amplitude in the range of 100 kHz-10 mHz (10^5-10^{-2} Hz). Equivalent circuit fitting was performed with the Zview (version 2.9c) program. All corrosion tests were performed in 3.5% NaCl aqueous solution.

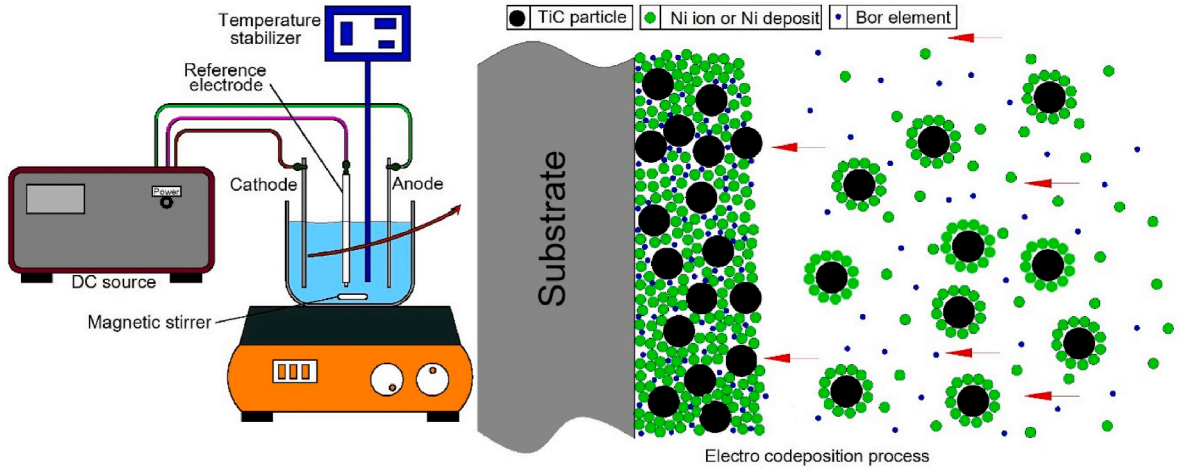

Fig. 1. Electrodeposition assembly and electroco-deposition process schema.

3. Result and discussion

3.1. Electrochemical analysis of TMAB effect in deposition baths

In Fig. 2, CV graphs of nanocomposite deposition baths with 7 g/l TiC bath concentration were given according to the change in TMAB bath concentration. The CV curve of the pure Ni and Ni–B alloy (3 g/l TMAB) deposition bath was also added to the figure. The peaks seen in the CV graphs from 1.2 V to 0 V in the cathodic direction are due to possible gas output. Then, it is seen that the current is at zero level in the curves in the range from 0 V to −0.85 V and it is understood that there is no reaction in this part. It occurs when the Ni metal starts to be deposited with rapid current increases seen from −0.85 V value, besides that it can be stated that H2 gas output contributes to this current increase. When examined in the anodic direction, the peaks seen from −0.5 V to around 0.6 V are formed during the dissolution of the deposited Ni metal back into the electrolyte. When the cathodic direction of the graphs is examined, it is seen that the deposition potential of the Ni–B alloy obtained as a result of adding TMAB to the bath does not change much compared to pure Ni. However, it is understood that the deposition potential shifts to the negative direction with the addition of TiC particles to the bath. It is thought that the change in this potential is due to the effect of TiC on the conductivity of the electrolyte. It can be stated that a higher deposition potential is needed due to TiC particles. The rate of increase in current density on the cathodic side decreased with the addition of TiC particle. In this case, it can be stated that there was a slight decrease in the amount of metal deposited.

When the anodic direction of the CV graphs is examined, it is observed that the anodic dissolution peak in the CV curve of the Ni–B alloy is quite high compared to the composite coatings. The addition of TiC caused a serious decrease in the height of the anodic dissolution peaks. In the anodic dissolution potential of nanocomposite coatings baths, there was a shift towards the positive side with the addition of TMAB and TiC particles compared to that of pure nickel bath, but there was no significant change in the dissolution peak heights. While the anodic dissolution peak was seen as more than one peak in the CV curve of pure nickel (It can be an indication that Ni metal is deposited in different phases), it stands out as a single peak in the CV curves of the nanocomposite coating and Ni–B alloy baths. When the TMAB bath concentration increase was evaluated in itself, it was seen that it did not affect the deposition and dissolution potential values. However, it is understood that the increase in TMAB concentration slightly increases the deposition current value on the cathodic side, and at the same time increases the dissolution peak, that is, the dissolution current value, on the anodic side. In this case, it can be stated that the increase in TMAB concentration contributes positively to the storage rate and process. The coating thicknesses given in section 3.4 also support this view. The coating thickness, which was around 10 μm in the bath with 3 g/l TMAB, was around 20 μm on average in the baths with 6 g/l and 9 g/l TMAB. This situation can be expressed as follows; when TiC particles are added to the bath, it shows a decreasing effect on the deposition rate of the base metal Ni, but it seems likely that the effect of TiC particles will decrease with the increase in the amount of TMAB in the bath and changing the structure of the electrolyte. A similar situation was obtained and explained in the crystal structure and microhardness analyzes given in sections 3.2 and 3.3. Although the current values increase with respect to the 3 g/l concentration, they appear to be the same for 6 and 9 g/l TMAB concentrations.

Electrochemical deposition of Ni–B alloy material, which is obtained by incorporating boron atoms into the main structure of pure nickel, is not yet a fully understood phenomenon. It is assumed that the boron element is included in the coating as a Ni–B alloy as a result of the TMAB adsorbing gradually on the surface of the formed nickel deposit, and then decomposes into elemental boron. Therefore, the amount of boron deposited with nickel can be determined by the distribution of TMAB in the bath, independent of the electrode potential. It is known that nickel is deposited as an alloy such as boron with some other elements such as phosphorus [45]**71**, molybdenum [46], tungsten [47] by electrochemical deposition method. In the literature, the term induced co-deposition is used for this type of co-deposition mechanism. Although there is a current flow in the system while pure nickel is being deposited, it is thought that the alloying side elements do not cause a current flow. Although it is not known exactly how this mechanism is, it is a widely studied subject in the literature [8, 48, 49]. In addition, the inclusion of TiC particles in the Ni–B main structure does not cause any current flow. The inclusion of second phase ceramic particles in a metal matrix in the electrodeposition method is expressed in the literature by the Guglielmi model. In this model, codeposition takes place in stages. Metal ions and micro or nano particles co-existing in the electrolyte interact with each other. As a result of this interaction, the particles are surrounded by metal ions, while the ions are adsorbed on the particles. Therefore, metal ions and particles begin to move together, and as the ions are pulled towards the cathode by the effect of the current, they also drag the particles together. Particles adhering to the cathode surface together with the ions first adsorb weakly. However, since the accumulation continues on the cathode surface, after a while, the particles are

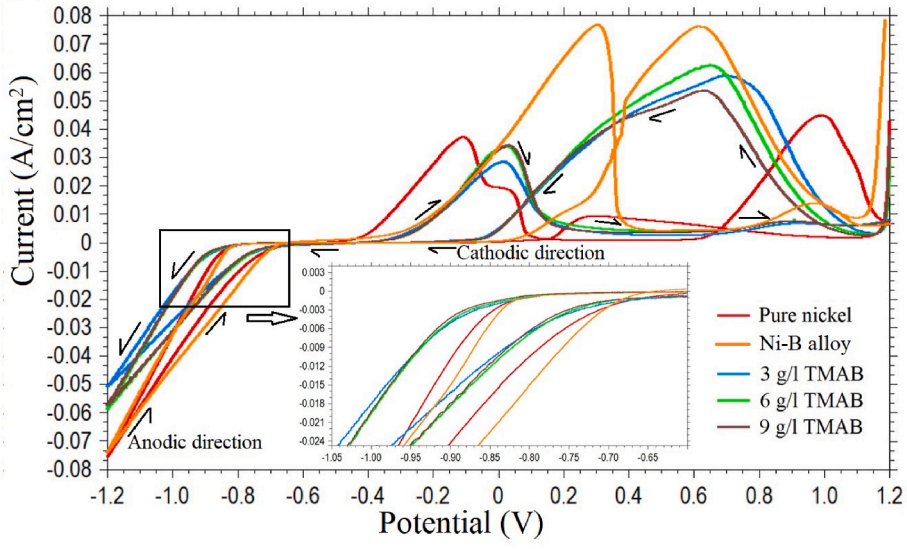

Fig. 2. CV graphs of nanocomposite deposition electrolytes with 7 g/l TiC bath concentration according to TMAB bath concentration change.

gradually buried and the accumulated metal is trapped in the main structure and the co-deposition process takes place. As long as the current acts, the coating layer gradually grows and the deposition process continues [50]. Electroco-deposition process schema is given in Fig. 1. Protsenko and Danilov [51] worked on a new model for the electrodeposition of composite coatings and claimed the opposite of the loose adsorption step specified in the Guglielmi model. According to the authors, the particles are irreversibly adhered to the surface after adsorbing to the cathode surface, and this is due to the relatively high interaction energy between the particles and the surface [50,51].

Onado et al. [52] reported that the deposition potential of pure nickel is 90 mV lower than that of the Ni–B alloy, and this may be due to the dissolution of TMAB in the bath and the adsorption of boron atoms on the electrode surface. Oriňáková et al. [53] stated that the addition of boron microparticles to the Watts-type nickel bath shifts the reduction potential to the more negative side. The authors attributed this to a reduction in metal reduction as a result of the effect of boron microparticles on the cathode surface. Ogihara et al. [49] stated that the addition of TMAB or DMAB to the bath did not significantly affect the reduction potential and a reducing current associated with the reduction of boron could not be observed.

3.2. Effect of TMAB bath concentration on crystal structure

When the XRD patterns of the Ni–B alloy coatings obtained as a result of adding TMAB to the Watts type electrolyte deposited in pure Ni in the literature are examined, the (200) peak of the pure nickel completely disappears and only the (111) peak remains. In addition to TMAB, it is frequently mentioned in previous studies that nickel-specific peaks become visible again in composite coatings with Ni–B alloy main structure obtained as a result of adding reinforcement particles to the bath [44,48,54–59]. In order to examine the effect of TMAB additive in the bath to alloy the nickel matrix with boron on the crystal structure, nanocomposite coatings were deposited at different TMAB concentrations and XRD patterns were obtained. XRD patterns of Ni–B/TiC nanocomposite coatings obtained at 3, 6 and 9 g/l TMAB bath concentrations were given in Fig. 3. In the figure, the TiC particle concentration was kept constant in each XRD pattern and the XRD patterns obtained from the samples deposited at 3, 5, 7 and 9 g/l bath concentrations were presented separately in order to better analyze the effect of TMAB. Besides nickel-specific (200), (111), (220), (311) and (222) peaks, (111) and (200) peaks belonging to TiC particles can be seen in XRD patterns. When Fig. 3 is examined closely, it was observed that the nickel-specific peaks (especially (111) and (200)) in the samples produced at a TiC bath concentration of 3 g/l first decrease and then increase with the increase in TMAB. It is possible to state that the intensity of nickel-specific peaks tends to increase with the increase in TMAB concentration in the XRD patterns of nanocomposite coatings produced at 5 g/l TiC particle concentration. The situation seems different at higher TiC bath particle concentrations. When the XRD patterns of the samples produced at 7 and 9 g/l TiC concentrations were evaluated, it was seen that the intensity of the nickel-specific peaks decreased and their widths increased with the increase in TMAB concentration. It can be seen from the results given in Table 2 that this situation also affects the crystal grain size. In the light of this information, the TMAB bath concentration acts differently at low particle concentrations, but differently at high particle concentrations, and it is understood that how complex the effects of each component are in electrodeposition baths. Normally, TMAB causes the structure of Ni–B alloy coatings to shift from crystalline to amorphous. However, at relatively low TiC concentrations such as 3–5 g/l, it is seen that the particles reduce the effect of TMAB in the bath, while at higher TiC particle concentrations, TMAB is more effective and changes the XRD patterns in this effect. According to these results, the effect of the bath concentration of TiC particles in the electrolyte decreases after a certain value due to possible agglomeration problems. From this interesting situation, it seems possible to conclude that TiC particles are more effective at low particle concentrations in the electrodeposition bath, whereas TMAB plays a more dominant role at high particle concentrations. The microhardness results given in sections 3.3 also support this view. The hardness of nanocomposite coatings produced at values higher than 5 g/l TiC particle bath concentration tends to decrease. It is possible to say that only a few studies have been

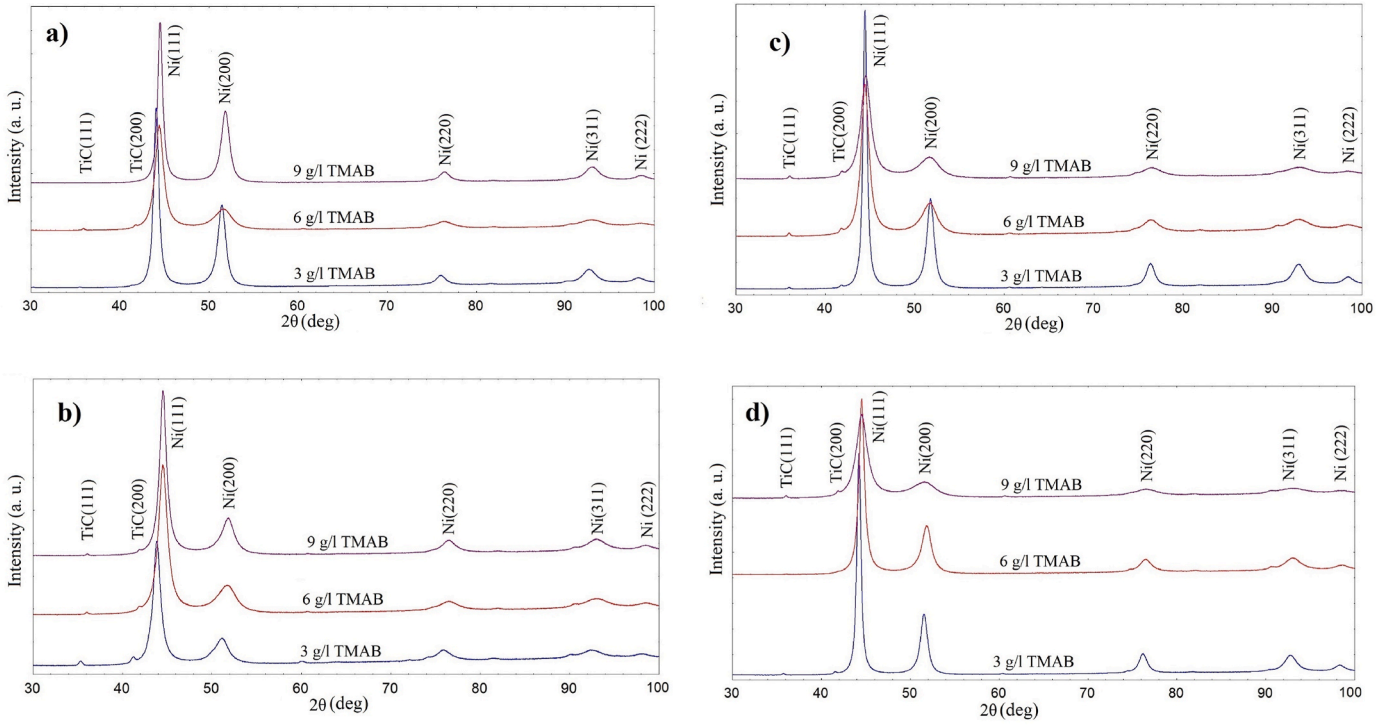

Fig. 3. The effect of TMAB concentration added to the bath on the crystal structure of Ni–B/TiC nanocomposite coatings (current density 50 mA/cm^2) a) 3 g/l TiC, b) 5 g/l TiC, c) 7 g/l TiC, d) 9 g/l TiC.

Table 2
Parameters obtained from XRD patterns of Ni–B/TiC nanocomposite coatings deposited at different TMAB concentrations.

Sample	2θ (deg)			FWHM-β (radian)			Average crystal grain size -D (nm)			Microstrain-ε x 10^{-3}		
	3 g/l TMAB	6 g/l TMAB	9 g/l TMAB	3 g/l TMAB	6 g/l TMAB	9 g/l TMAB	3 g/l TMAB	6 g/l TMAB	9 g/l TMAB	3 g/l TMAB	6 g/l TMAB	9 g/l TMAB
3 g/l TiC	44	44.4	44.4	0.01186	0.01913	0.01152	13.2	8.2	13.6	7.3	11.7	7.1
5 g/l TiC	43.9	44.5	44.5	0.01680	0.01972	0.01459	9.3	7.9	10.7	10.4	12	8.9
7 g/l TiC	44.4	44.4	44.6	0.00928	0.01747	0.02189	16.8	8.9	7.2	5.7	10.7	13.3
9 g/l TiC	44.2	44.5	44.5	0.00945	0.01262	0.02358	16.5	12.4	6.6	5.8	7.7	14.4

conducted in the literature investigating the effects of TMAB bath concentration on Ni–B alloy-based composite coatings. Li et al. **[60]** investigated the effect of TMAB bath concentration on XRD patterns in Ni–B/Al_2O_3 nanocomposite coatings. The authors stated that with the increase in TMAB concentration, the intensity of the (111) and (200) peaks specific to pure nickel decreased and disappeared, and they stated that there was a direct relationship between the increase of TMAB and the growth of amorphous structure in nanocomposite coatings. In another study, Zhang and Li [8] examined the crystal structure of Ni–B/SiC nanocomposites in order to investigate the effect of TMAB. The authors demonstrated that with the increase in the amount of TMAB in the bath, the width of the (111) peak of nickel increased and the coating structure changed towards amorphous structure. According to the authors, the presence of large peaks can be explained by the fact that the Ni–B coatings are a solid solution of the element boron in the fcc nickel lattice.

In Table 2, the crystal grain size and microstrain parameters obtained from the XRD patterns of Ni–B/TiC nanocomposite coatings deposited at different TMAB bath concentrations were given in order to analyze the TMAB effect. While calculating these parameters, the peaks with the highest intensity in the XRD pattern were used. The crystal grain size was calculated as 42.6 nm for pure Ni and 8.7 nm for Ni–B. When Table 2 was examined, it was seen that the effect of TMAB bath concentration on the mean crystal grain size was affected by the TiC particle bath concentration. In the samples produced at 3 and 5 g/l TiC bath concentrations, with the increase in TMAB, the crystal grain size first decreases and then increases again. It was seen that the values of the bath with 9 g/l TMAB in these baths were higher than the values of the bath with 3 g/l TMAB, with the increase. In samples with 7 and 9 g/l TiC bath concentrations, the average crystal grain size tends to decrease with the increase in TMAB. The addition of TMAB to the pure nickel-produced Watts-type bath has the effect in the reduction of the crystal grain size seriously, then the crystal grain size tends to increase slightly with the addition of TiC particles to the Ni–B alloy produced bath [44, 48, 54–59]. However, with the increase of the TMAB concentration in the bath again, TMAB becomes dominant again and plays a very effective role in reducing the crystal grain size. In Table 2, the change of microstrain values with the increase in TMAB was given. With the increase in TMAB bath concentration at 3 and 5 g/l TiC concentrations, the microstrain values first increase and then decrease. However, at higher TiC bath concentrations (7 and 9 g/l), these values tend to increase continuously with the increase in TMAB.

Relative texture coefficient (RTC) values of Ni–B/TiC nanocomposite coatings are given in Table 3. In addition, RTC values of pure Ni and Ni–B alloy (3 g/l TMAB) are given for comparison. It can be seen that the preferential orientation of the pure Ni coating is parallel to the (200) plane. In the Ni–B alloy, unlike pure Ni, the orientation in the (200) plane decreased significantly and the orientation in the (111) and (220) planes increased. The Ni–B alloy has a random orientation relative to pure Ni. When the RTC values of nanocomposite coatings are examined, it is seen that the preferential orientation is concentrated in the (111) plane. For the (111) plane, there is an increase and decrease with the increase in TMAB at low TiC concentrations, while a slight decrease is observed at high TiC concentrations. However, it can be said that the RTC values are close to each other. In the (200) plane, a decrease is observed with the increase in TMAB at high TiC bath contents, while the opposite increase is observed in the (220) plane. When nanocomposite coatings are compared with Ni–B alloy, it is observed that the RTC values of the (111) plane are similar, while the RTC value of the (200) plane increases and the (220) RTC value decreases.

3.3. Effect of TMAB bath concentration on microhardness

The effect of TMAB bath concentration change on microhardness was investigated holding the current density constant at 50 mA/cm^2 in all samples. The microhardness of the stainless steel substrate was measured at 203 HV, the microhardness of the pure Ni coating was around 290 HV, and the microhardness of the Ni–B alloy was around 400 HV. In Fig. 4, the effect of TMAB concentration on the hardness of Ni–B/TiC nanocomposite coatings was given. As can be seen from the figure, when the TMAB concentration in the bath was increased to 6 g/l, the microhardness values first increased and then decreased for 3, 5, 7 g/l particle concentrations. However, a continuous decrease was observed with the increase of TMAB at 9 g/l TiC particle concentration. In addition, the hardness values at 9 g/l TMAB concentration were lower than those at 3 g/l TMAB concentration. In Ni–B alloys, with the addition of TMAB to the bath, boron atoms were included in the nickel main structure and cause an increase in hardness [61]. According to this information, although an increase in hardness can be expected with an increase in TMAB, the decrease in microhardness values higher than 6

Table 3
Relative texture coefficient values (Ni–B alloy, 3 g/l TMAB).

Sample	RTC (111)			RTC (200)			RTC (220)		
	3 g/l TMAB	6 g/l TMAB	9 g/l TMAB	3 g/l TMAB	6 g/l TMAB	9 g/l TMAB	3 g/l TMAB	6 g/l TMAB	9 g/l TMAB
3 g/l TiC	38.2	45.42	38.3	42.3	24.05	41.73	19.5	30.53	19.92
5 g/l TiC	38.14	45.25	43.61	23.02	23.2	25.19	38.83	31.56	31.2
7 g/l TiC	44.72	42.03	41.36	30.67	23.55	23.38	24.65	34.42	35.25
9 g/l TiC	43	42.8	41.87	28.68	29.5	22	28.3	27.6	36.1
Pure Ni	2.48			97.1			0.44		
Ni–B alloy	40.75			14.7			44.52		

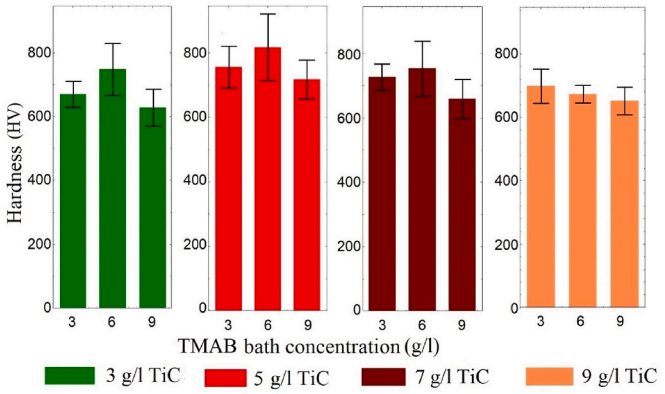

Fig. 4. The effect of TMAB bath concentration on the hardness of Ni–B/TiC nanocomposite coatings.

g/l TMAB concentration is an indicator of how TiC particles affect the characteristic properties of the bath. In comparison with TiC particle concentrations, it was seen that the highest hardness values were obtained at 5 g/l TiC particle concentration. In this case, it can be said that the optimum particle concentration value in terms of microhardness is 5 g/l. The highest hardness values after 5 g/l particle concentration were obtained at 7 g/l particle bath concentration. In terms of TMAB effect, the optimum value stands out as 6 g/l, but this is not the case at a TiC particle concentration of only 9 g/l. Because at 9 g/l TiC particle concentration, the highest hardness value was obtained at 3 g/l TMAB concentration. In general, the highest hardness value was obtained with 817 HV at 6 g/l TMAB and 5 g/l TiC bath concentrations. The lowest hardness value was obtained at 628 HV and 9 g/l TMAB and 3 g/l TiC particle concentration. Li et al. [60] investigated the effects of TMAB bath concentration change on the microhardness of coatings in their study of Al_2O_3 reinforced Ni–B based nanocomposites. According to their results, the authors stated that the hardness of the coating increased rapidly up to a certain TMAB concentration value (2 g/l), and after this value, there was a slight decrease in the hardness. The authors stated that the relationship between TMAB concentration and hardness was complex. Another issue related to the hardness results is that when the measurement load (500gr; such a load was preferred for the full formation of the trace to be able to make a proper measurement) given in the experimental part in section 2 and the coating thicknesses seen in the cross-sectional SEM pictures are compared, the possibility that the hardness results may be affected by the substrate according to Buckle's one-tenth rule comes to mind. However, we think that this effect is negligible. In the literature, it is stated that Buckle's one-tenth rule is not a universal and definite rule. And this rule is based on experimental results on some materials. In addition, it is stated that studies are carried out on materials that do not comply with this rule, especially amorphous, nanostructured and polycrystalline materials deviate from Buckle's one-tenth rule and the indentation depth rule between 0.2t and 0.66t can be applied in such materials [62–65]. Considering that our Ni–B/TiC nanocomposite coating is a new type of nanostructured material, we predict that the amount of influence on the substrate in hardness measurements will be negligible. In addition, when compared with the hardness results obtained in similar Ni-based electrodeposited composite coating systems in which TiC is used as a reinforcement, it is seen that our hardness results are quite acceptable and reasonable [12,30,59,66–68].

3.4. Morphology and content analysis of the effect of TMAB bath concentration

Morphology and content analyzes of Ni–B/TiC nanocomposite coatings produced at different TMAB bath concentrations were performed with SEM device in order to analyze the effect of boron source TMAB added to the electrolyte. The current density value of the samples was chosen as 50 mA/cm^2 and the TiC particle bath concentration was chosen as 5 g/l whose TMAB effect was examined. Surface SEM images of pure Ni and Ni–B alloy are presented in Fig. 5 for comparison purposes. It can be seen from the surface image of pure Ni that it has a pyramidal structure, while the surface of the Ni–B alloy is flatter and consists of sparse circular mounds. Ni–B/TiC nanocomposite coatings, on the other hand, have a very different surface morphology than pure Ni and Ni–B alloys. In Fig. 6, surface morphology images of nanocomposite samples produced at 3, 6 and 9 g/l TMAB bath concentrations were given at 5000 and 100000 magnifications. As can be seen from Fig. 6, a cauliflower-like structure stands out. At higher magnifications, these structures resemble bunches of grapes. Although it was seen that the change in TMAB bath concentration does not cause a serious change on the surface morphology, it was observed that the diameters of the spherical shaped formations slightly increase with the increase in TMAB. Zhang and Li [8] investigated the effect of TMAB on the morphology of Ni–B/SiC nanocomposite coatings and reported that the surface gained a nodular and spherical appearance with the increase of TMAB. Apart from this, we could not find any other study examining the effect of TMAB on morphology and element content in the literature.

EDS content analyzes of nanocomposite coatings deposited at 3, 6 and 9 g/l TMAB bath concentrations were given in Fig. 7. In the content analysis, the presence of the peaks of Ni, B, Ti and C elements that make up the nanocomposite coating can be seen and it is seen that the B element in the coating increases with the increase in TMAB bath concentration. Although the amount of B in the 9 g/l TMAB bath showed a very limited decrease, it is higher than the 3 g/l TMAB bath. If the amount of TiC in the nanocomposite coating is interpreted through the obtained Ti element percentages, it seems possible to say that the amount of particles decreases with the increase in TMAB concentration, which is expected with the increase in TMAB. As previously stated in CV and XRD comments, the increase in TMAB suppresses the effect of TiC particles. Ganji et al. [69], in the EDS analyzes of their study on Ni–Fe/TiC nanocomposite coatings, similar to our results, the Ti and C contents were reflected in the analyzes at quite different ratios by weight. It can be attributed that this interesting situation arises from the nature of TiC particles and is reflected in the analysis in this way.

Elemental mapping analysis obtained from the surface of the nanocomposite coating produced at 6 g/l TMAB bath concentration was given in Fig. 8. As seen in the results obtained, it was understood that TiC particles and boron element were successfully included in the main structure. It can be seen that the Ti and C elements, which form the reinforcement particles, and the B elements, which form the alloy, show a homogeneous distribution in the main structure.

In Fig. 9, cross-sectional SEM images of nanocomposite coatings deposited at 3 different TMAB concentrations were given. It was observed that the coatings were partially separated from the substrate due to the forces and vibrations that occur during the cutting of the samples. In addition, there were parts where the coatings adhere well to the substrate material. Although the coating thicknesses vary from place to place along the section line, it was measured around 5–10 μm in the sample with 3 g/l TMAB, while it was measured around 15–20 μm in the samples deposited in the baths with 6 and 9 g/l TMAB.

Linear EDS analysis results of 6 and 9 g/l TMAB samples taken over the cross-sectional surface were given in Fig. 10. The results showed that the presence of Ti, C and B elements from the surface to the bottom of the coating and were evidence of successful deposition of the composite coating. In Fig. 11, the results of elemental mapping analysis taken from a certain rectangular region on the cross-sectional image of the nanocomposite sample with 6 g/l TMAB bath concentration were given. As can be seen from the results obtained, TiC reinforcement nanoparticles and the boron element were successfully deposited in a homogeneous distribution from the surface to the bottom of the coating. These mapping analysis intensify the view that a successful nanocomposite coating structure has been obtained.

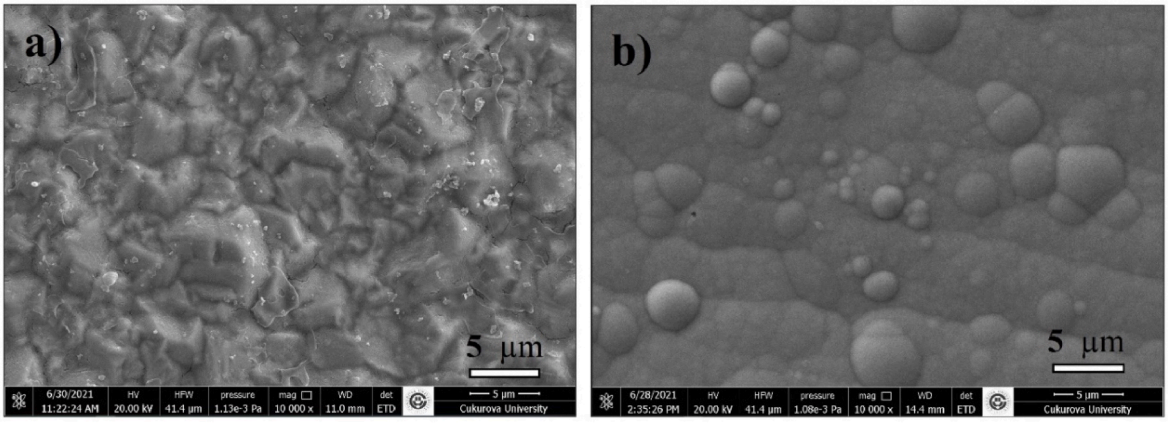

Fig. 5. Surface morphology of a) pure Ni, b) Ni–B alloy coatings.

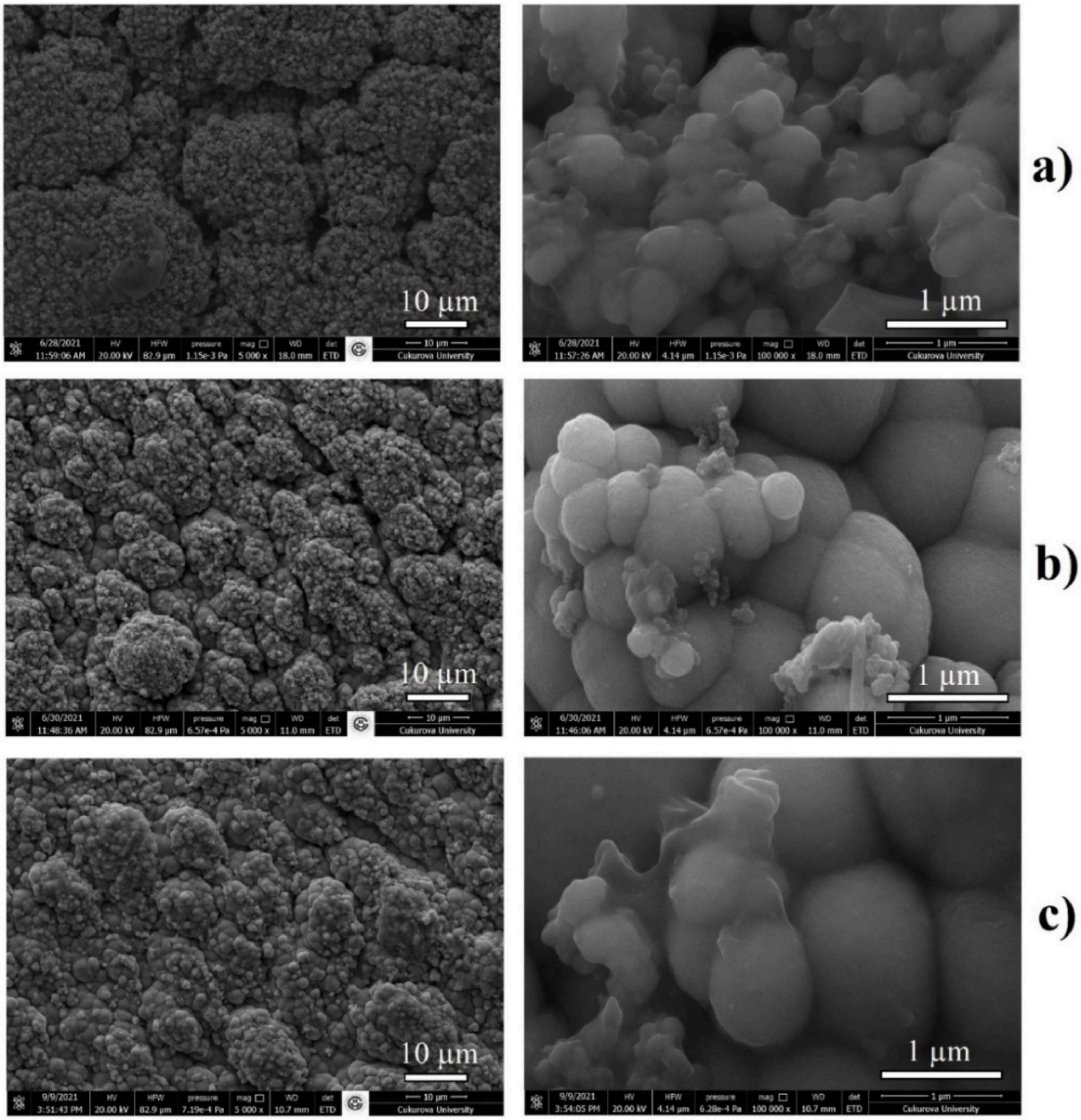

Fig. 6. Effect of TMAB bath concentration on the surface morphology of Ni–B/TiC nanocomposite coatings; a) 3 g/l, b) 6 g/l, c) 9 g/l TMAB bath concentration (50 mA/cm^2 current density and 5 g/l TiC bath concentration, 5000 magnification on the left, 100000 magnification on the right).

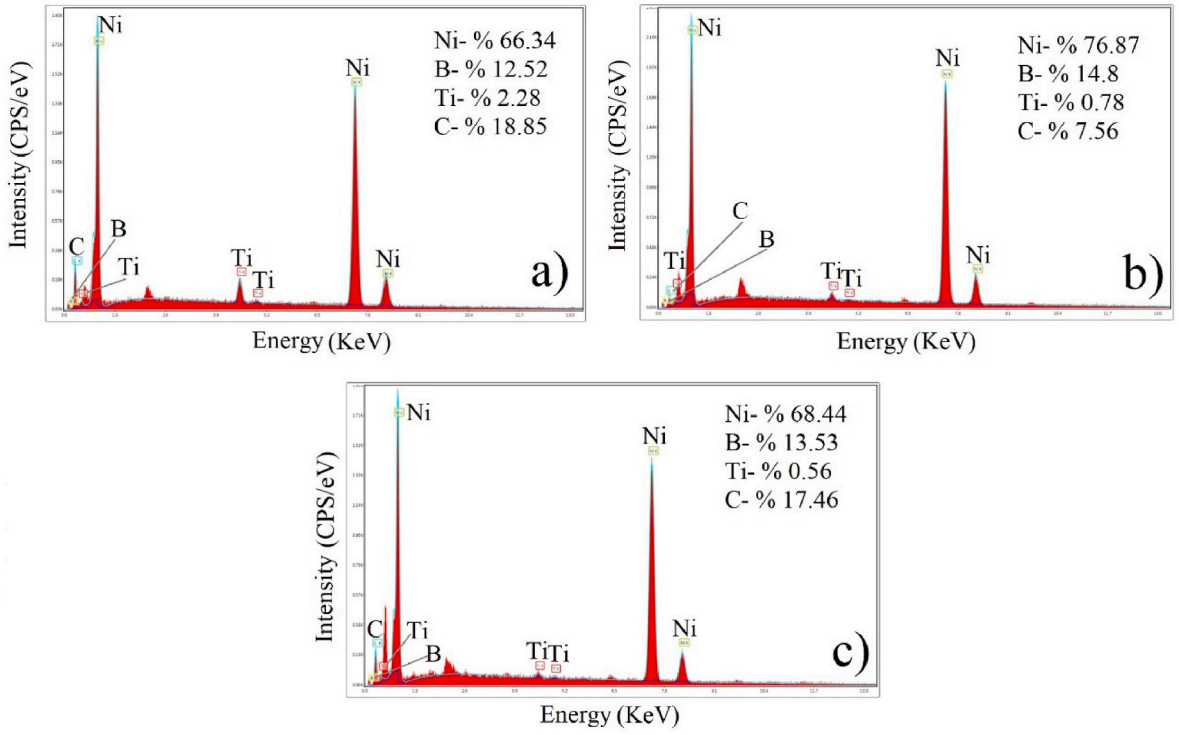

Fig. 7. Surface EDS content analysis of Ni–B/TiC nanocomposite coatings produced at different TMAB bath concentrations a) 3 g/l, b) 6 g/l and c) 9 g/l TMAB.

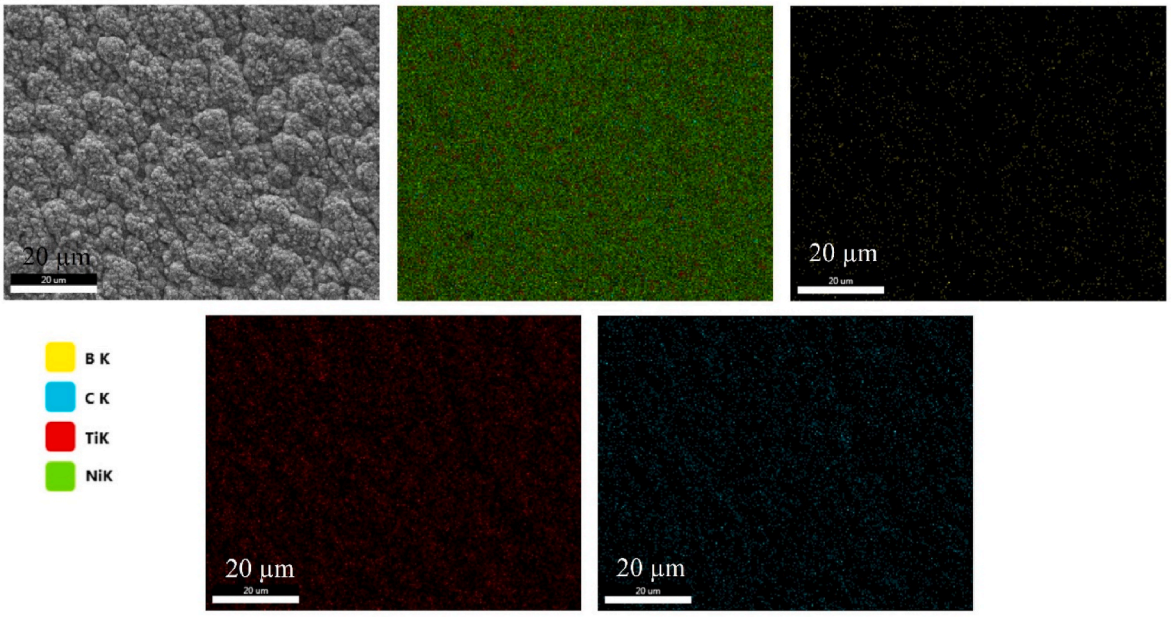

Fig. 8. Elemental mapping analyzes of Ni–B/TiC nanocomposite coating with 6 g/l TMAB bath concentration.

3.5. *Effect of TMAB bath concentrations on corrosion behaviors*

In Ni–B/TiC nanocomposite coatings, the effect of TMAB bath concentrations on corrosion resistance was investigated over 12 g/l TiC bath concentration, which showed the best corrosion performance among 3–12 g/l TiC particle concentrations [70]. Tafel curves of the effect of TMAB bath concentration on the corrosion performance of Ni–B/TiC nanocomposite coatings were given in Fig. 12. Table 4 presents the data obtained from the Tafel curves. In addition, corrosion analysis results of stainless steel substrate, pure Ni and Ni–B alloy are given in Fig. 12 and Table 4 for comparison purposes. When the figure is examined, it is seen that the corrosion performance of Ni–B/TiC nanocomposite coatings is much better than the stainless steel substrate, pure Ni and Ni–B alloy. When nanocomposite coatings are examined according to different TMAB concentrations, it was seen that the increase in TMAB bath concentration first causes a slight decrease in corrosion performance, and then it reaches better levels than the case with 3 g/l TMAB bath concentration. In the evaluation of corrosion current, compared to the sample with 3 g/l TMAB bath concentration, a corrosion current increase of around 13% was observed in the sample with 6 g/l TMAB,

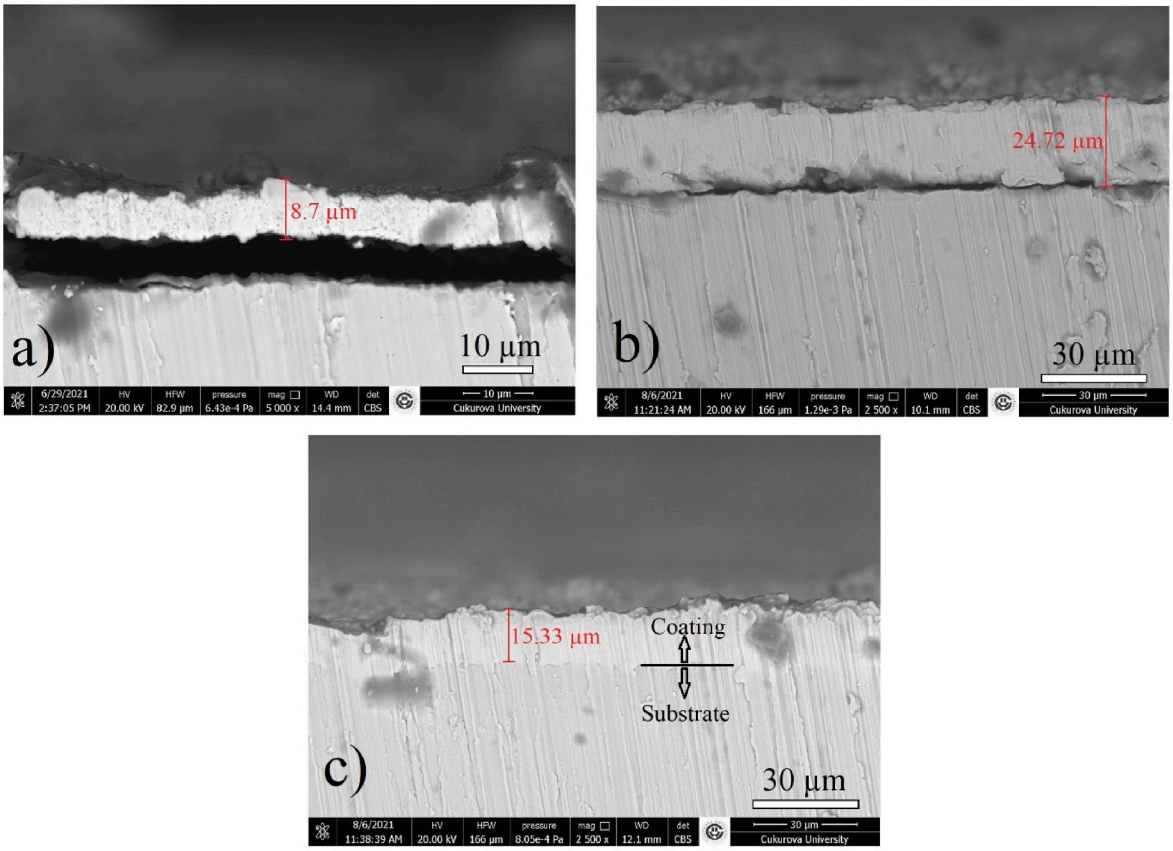

Fig. 9. Cross-sectional SEM images of Ni–B/TiC nanocomposite coatings produced at different TMAB bath concentrations a) 3 g/l, b) 6 g/l and c) 9 g/l TMAB.

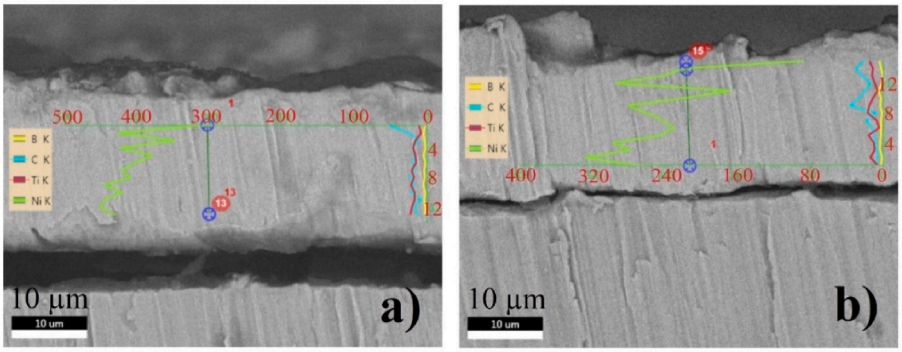

Fig. 10. Linear EDS analyzes taken from the cross-sectional areas of Ni–B/TiC nanocomposite coatings produced at different TMAB bath concentrations, a) 6 g/l TMAB, b) 9 g/l TMAB.

while a decrease in corrosion current of around 44% was observed in the sample with 9 g/l TMAB. In terms of corrosion potentials, it is seen that the samples with 3 and 9 g/l TMAB bath concentrations are very close to each other, while the sample with 6 g/l TMAB is on the more negative side. In the light of these data, it can be stated that the increase in TMAB bath concentration causes an improvement in corrosion performance. In the literature, it is reported that there is a decrease in corrosion performance as a result of the inclusion of boron atoms in the nickel main structure with TMAB added to the bath, and it is stated that the reason for this decrease may be due to cracks larger or smaller than micron size due to the tense internal structure of the Ni–B alloy [56,57,71,72]. However, with the addition of TiC particles to the bath, the nature of the electrochemical bath changes and TMAB, which adversely affects the corrosion in the Ni–B alloy produced bath, can cause positive effects in terms of corrosion in the nanocomposite produced bath. In other words, TiC particles seriously affected the structure of the coating. These results show that the analysis of electrochemical production baths are very complex and each component added to the bath has very serious effects. An increase in TMAB concentration causes a decrease in crystal grain size, and the improvement of corrosion resistance may be associated with a decrease in crystal grain size. Because fine-grained materials have a denser structure, it is expected that they are more resistant to corrosion [60].

EIS graphs obtained to analyze the effect of TMAB bath concentrations on the corrosion resistance of Ni–B/TiC nanocomposite coatings are given in Fig. 13. In the figure, the curves of pure Ni, Ni–B alloy and stainless steel substrate are given for comparison, and it is observed that the corrosion performance of nanocomposite coatings is much better

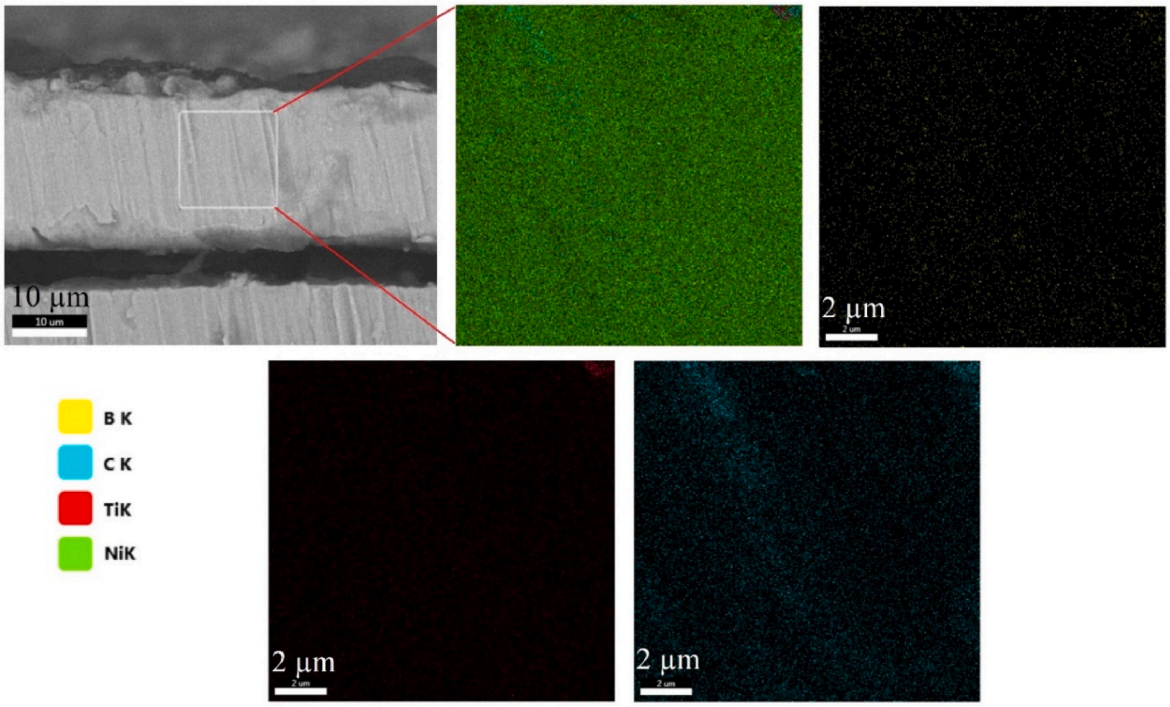

Fig. 11. Elemental mapping analysis of a specific region on the cross-sectional SEM image of the Ni–B/TiC nanocomposite coating produced at 6 g/l TMAB bath.

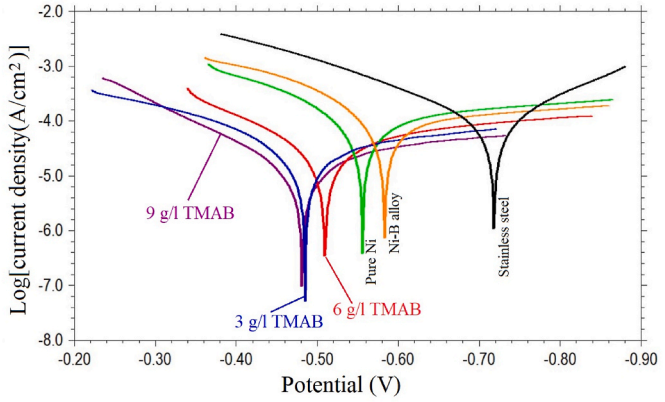

Fig. 12. Tafel curves of stainless steel substrate, pure Ni, Ni–B alloy and Ni–B/TiC nanocomposite coatings with different TMAB bath concentration (TiC bath concentration 12 g/l, current density 50 mA/cm^2, Ni–B alloy 3 g/l TMAB).

Table 4
Tafel data of samples.

Samples	E_{cor} (V)	I_{cor} (A)	Corrosion rate (mm/year)
Stainless steel substrate	−0.718	10.7×10^{-5}	4.42
Pure Ni	−0.556	10.5×10^{-5}	4.31
Ni–B alloy (3 g/l TMAB)	−0.583	12.47×10^{-5}	5.13
3 g/l TMAB Ni–B/TiC nanocomposite coating	−0.485	2.83×10^{-5}	1.16
6 g/l TMAB Ni–B/TiC nanocomposite	−0.509	3.18×10^{-5}	1.31
9 g/l TMAB Ni–B/TiC nanocomposite	−0.481	1.59×10^{-5}	0.65

than these samples. Examining the Nyquist graph given in Fig. 13 (a), first a decrease and then an increase occurred in the corrosion performance with the increase in TMAB bath concentration. As can be seen from the figure, the sample produced in the 9 g/l TMAB concentration bath seems closer to the virtual axis and more inclusive than the others, in other words, the capacitive loop diameter is larger in this sample. In the impedance modulus and bode graphs given in Fig. 13 (b) and (c), the bath with 9 g/l TMAB concentration has the highest values and exhibited the best corrosion resistance performance. In Fig. 13 (b), the samples exhibited a high impedance modulus in the low frequency region. This indicates that the corrosion protection mechanism of nanocomposite coatings is capacitive. It is known that the capacitance character can improve the protective ability of the coating by preventing the transport of corrosive substances throughout the coating. The capacitive feature increases the chemical stability of protective coatings [16,60]. In the high frequency region of the same graph, the impedance modulus values of the curves of the samples decreased and the curves were very close to each other. In this case, it can be said that the samples do not differ from each other in terms of corrosion activity in the high frequency region.

In Table 5, the data obtained from the equivalent electrical circuit fitting curves were presented and it was seen that the results were compatible with each other. For the fitting process, the equivalent electrical circuit with warburg given in Fig. 13 (d) was used. In the electrical equivalent circuit, “Rs” represents the solution resistance, “Rp” and “W” represents the total resistance of the coating, and CPE represents the stationary phase element of the coating. CPE is used to compensate for the inhomogeneity of systems due to factors such as roughness, porosity, reactivity, potential and current distribution at the interface or electrode geometry where corrosion occurs [73]. In Table 5, “Yo” and “n” represent the magnitude and phase exponent of the CPE capacitance, and the capacitor with phase exponent of 1 is an ideal CPE. W–P represents the slope of the warburg section. Considering the states of all the curves, the need to add a Warburg impedance to the electrical circuit has arisen in order to achieve a similar curve. The Warburg impedance element shows that the electrochemical processes at the interface of the coating with the solution are under diffusion control as

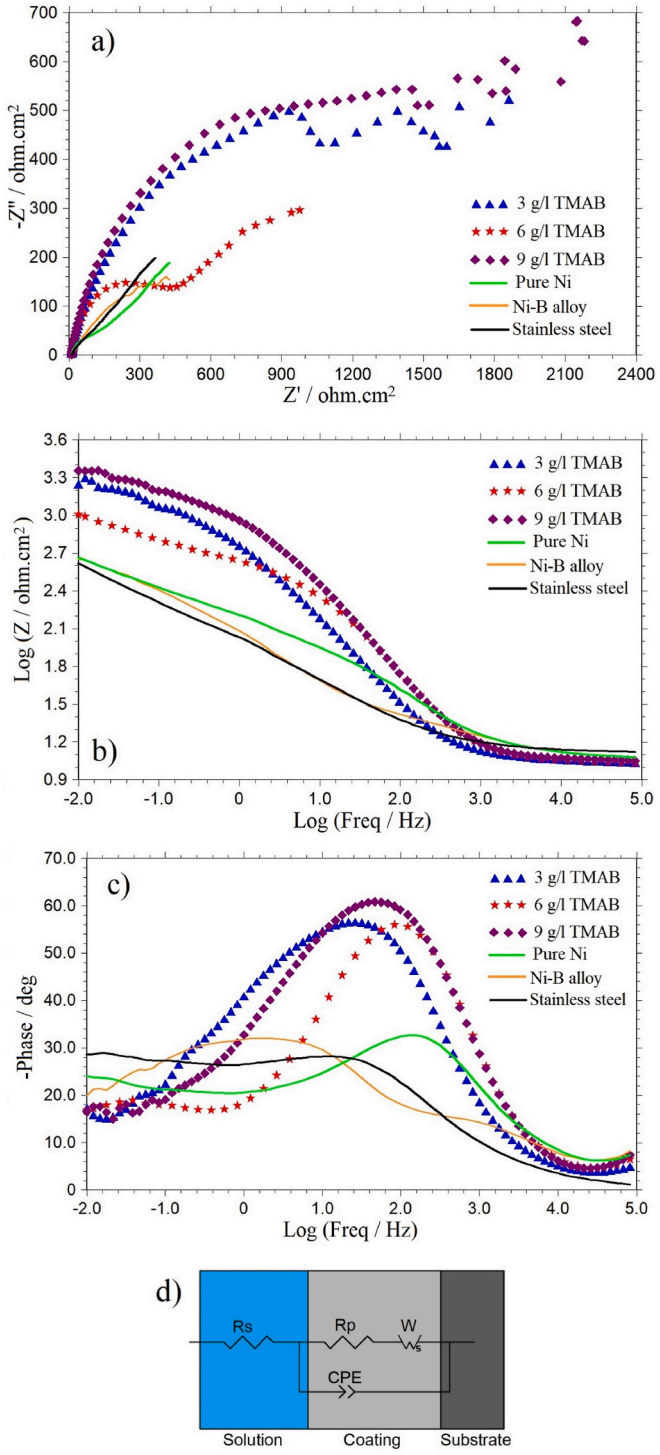

Fig. 13. EIS plots of stainless steel substrate, pure Ni, Ni–B alloy and Ni–B/TiC nanocomposite coatings with different TMAB bath concentration (TiC bath concentration 12 g/l, current density 50 mA/cm^2, Ni–B alloy 3 g/l TMAB) a) Nyquist, b) impedance modulus, c) bode, d) equivalent electrical circuit.

well as being kinetic controlled [74]. According to the data obtained, it was displayed that the sample with the highest Rp and W total resistance value, with 9 g/l TMAB bath concentration had the best corrosion resistance. It is also noticed that all nanocomposite coatings exhibit much higher resistance values than pure Ni, Ni–B alloy and stainless steel substrate. Li et al. [60] reported that the increase in TMAB concentration in the bath has a negative effect on corrosion resistance of Al_2O_3 reinforced Ni–B based composite coatings. In this case, it was

Table 5
EIS equivalent circuit analysis of stainless steel substrate, pure Ni, Ni–B alloy and Ni–B/TiC nanocomposite coatings with different TMAB bath concentration (TiC bath concentration 12 g/l, current density 50 mA/cm^2, Ni–B alloy 3 g/l TMAB).

Sample	Rs (Ω. cm^2)	Rp (Ω. cm^2)	Yo (Ω^{-1} s^n cm^{-2})	n	W (Ω. cm^2)	W–P
Stainless steel	12	70	0.0054	0.59	900	0.36
Pure Ni	11	150	0.0027	0.53	1000	0.36
Ni–B alloy[a]	11	880	0.01279	0.43	–	–
3 g/l TMAB	11	1700	0.0018	0.62	1100	0.47
6 g/l TMAB	11	300	0.0006	0.78	1400	0.31
9 g/l TMAB	11	1000	0.0012	0.75	2200	0.3

[a] Equivalent electrical circuit without warburg impedance is used for Ni–B alloy.

revealed that TMAB bath concentrations in different particle types have different effects on corrosion.

Corrosion generally starts from the surface and progresses through the surface defects such as micro or nanopores, pits or cracks to the interior of the coating. The higher the amount of these defects, the higher the corrosion rate. Nanoparticles added to the main structure in the form of metal or alloy cause the formation of many core centers during the growth of the crystals and provide a fine-grained, homogeneous, tight and dense (compact) structure. Moreover, nanoparticles can be effectively absorbed into micro-defects and cracks and play an important role in filling the defects. This improves the compactness level of the coating and prevents the corrosion medium from penetrating the coating. Since these nanoparticles, which are generally ceramic, are chemically stable and electrically insulating, they act as a barrier between the substrate and the solution in corrosive environments [29].

The addition of reinforcement particles to the main structure reduces the active areas on the coating surface and prevents taking place hydrogen formation reactions. The inclusion of reinforcement TiC particles in the Ni–B main structure affects the processes of both anodic and cathodic reactions, that is, suppresses these reactions. This situation affects the cathodic hydrogen formation reactions as well as the anodic dissolution reactions [75]. Another explanation for this issue is that the reinforcement particles, which are well located and distributed at the grain boundaries during the deposition process, reduce the defects in the coating. This makes the coating denser and non-porous, thus increasing the corrosion resistance [76]. It can be thought that the improvement in corrosion resistance of Ni–B/TiC nanocomposite coatings depends on the factors mentioned above.

4. Conclusions

In this study, TiC particle reinforced Ni–B alloy based composite coatings were deposited on a stainless steel substrate by electrodeposition method. The developing properties of the obtained nanocomposite coatings were analyzed by various methods in terms of the effects of the change in TMAB bath concentration which is a boron alloying source. Obtained results were presented below.

- It was observed that the addition of TMAB to the electrochemical bath did not have a significant effect on the deposition or dissolution potentials. However, it has been understood that the increase in TMAB in the bath has a positive effect on increasing the amount of deposition.
- Considering the effect of TMAB on the crystal structure of the coatings, especially in terms of crystal grain size, it is seen that TiC particles are more effective at low particle concentrations in the electrodeposition bath, while TMAB plays a more dominant role at high particle concentrations.
- With the increase in TMAB bath concentration, the microhardness values of the nanocomposite coatings first increased and then

decreased. The highest hardness value was obtained with 817 Hv at 6 g/l TMAB and 5 g/l TiC bath concentrations.

- It was observed that the surface morphologies of the nanocomposite coatings had a cauliflower-like structure. Although it is seen that the change in TMAB bath concentration does not cause a very serious change on the surface morphology, it is observed that the diameters of spherical shaped formations slightly increase with the increase in TMAB. In addition, it is possible to state that while the amount of B increases with the increase in TMAB, the amount of TiC particles tends to decrease.
- It was observed that the increase TMAB bath concentration contributed positively to the corrosion resistance. In terms of corrosion current, a decrease of around 44% was obtained in the sample with 9 g/l TMAB compared to the sample with 3 g/l TMAB bath concentration.
- It has been determined that Ni–B/TiC nanocomposite coatings are in a much better situation in terms of corrosion and hardness than pure Ni, Ni–B alloy and stainless steel substrate.

Declaration of competing interest

The authors declare that they have no known competing financial interests or personal relationships that could have appeared to influence the work reported in this paper.

Acknowledgements

The authors thank to the Scientific Research Projects of Çukurova University for financial support of this research (ÇU-BAP, **Proje ID:** 12868).

References

[1] M. Mirak, A. Akbari, Microstructural characterization of electrodeposited and heat-treated Ni-B Coatings, Surf. Coating. Technol. 349 (2018) 442–451.
[2] M.S. Mehr, A. Akbari, E. Damerchi, Electrodeposited Ni-B/SiC micro- and nano-composite coatings: a comparative study, J. Alloys Compd. 782 (2019) 477–487.
[3] T.G. Schuh, C.A. Nieh, H. Iwasaki, The effect of solid solution W additions on the mechanical properties of nanocrystalline Ni, Acta Mater. 51 (2) (2003) 431–443.
[4] A. Tozar, İ.H. Karahan, Effect of octylphenyl ether group nonionic surfactant on the electrodepositon of the hexagonal boron nitride reinforced Ni-B matrix composite coatings, Surf. Coating. Technol. 381 (2019), 125131.
[5] K.H. Lee, D. Chang, S.C. Kwon, Properties of electrodeposited nanocrystalline Ni-B alloy films, Electrochim. Acta 50 (2005) 4538–4543.
[6] Y. Liang, Y.S. Li, Q.Y. Yu, Y.X. Zhang, W.J. Zhao, Z.X. Zeng, Structure and wear resistance of high hardness Ni-B coatings as alternative for Cr coatings, Surf. Coating. Technol. 264 (2015) 80–86.
[7] D. Li, B. Li, S. Du, W. Zhang, Synthesis of a novel Ni–B/YSZ metal-ceramic composite coating via singlestep electrodeposition at different current density, Ceram. Int. 45 (2019) 24884–24893.
[8] W. Zhang, B. Li, Influence of electrodeposition conditions on the microstructure and hardness of Ni-B/SiC nanocomposite coatings, Int. J. Electrochem. Sci. 13 (2018) 3486–3500.
[9] U.S. Waware, A.M.S. Hamouda, B. Bajaj, T. Borkar, A.K. Pradhan, Synthesis and characterization of electrodeposited Ni-B-Tl_2O_3 composite coatings, J. Alloys Compd. 769 (2018) 353–359.
[10] C.T.J. Low, R.G.A. Wills, F.C. Walsh, Electrodeposition of composite coatings containing nanoparticles in a metal deposit, Surf. Coating. Technol. 201 (2006) 371–383.
[11] N.S. Qu, K.C. Chan, D. Zhu, Pulse co-electrodeposition of nano Al_2O_3 whiskers nickel composite coating, Scripta Mater. 50 (8) (2004) 1131–1134.
[12] M. Karbasi, N. Yazdian, A. Vahidian, Development of electro-co-deposited Ni–TiC nano-particle reinforced nanocomposite coatings, Surf. Coating. Technol. 207 (2012) 587–593.
[13] M.G. Hosseini, S. Ahmadiyeh, A. Rasooli, Pulse plating of Ni–B/WC nanocomposite coating and study of its corrosion and wear resistance, Mater. Sci. Technol. 35 (10) (2019) 1248–1256.
[14] Y. Zhang, S. Zhang, Y. He, H. Li, T. He, T. Fan, H. Zhang, Mechanical properties and corrosion resistance of pulse electrodeposited Ni-B/B_4C composite coatings, Surf. Coating. Technol. 421 (2021), 127458.
[15] H.H. Sheu, Q.Y. Wang, P.C. Huang, A.Y. Cheng, Y.M. Liu, K.H. Hou, M.D. Ger, Effect of trimethylamine borane (TMAB) on the corrosion resistance and mechanical properties of nickel-based composite coatings, Int. J. Electrochem. Sci. 16 (2021), 21049.
[16] A. Tozar, Investigating the hexadecylamine as a new nonionic surfactant candidate for electrodeposition of wear-resistant metal-matrix composites, Surf. Eng. 36 (9) (2020) 990–999.
[17] A. Tozar, İ.H. Karahan, Investigation of the mechanical properties of Ni-B/hBN composite coatings electrodeposited in presence of CTAB as the surfactant, Mater. Res. Express 6 (12) (2019), 126598.
[18] S. Ahmadiyeh, A. Rasooli, M.G. Hosseini, Ni–B/SiC nanocomposite coating obtained by pulse plating and evaluation of its electrochemistry and mechanical properties, Surf. Eng. 35 (10) (2019) 861–872.
[19] F. Doğan, E. Duru, M. Uysal, H. Akbulut, S. Arslan, Tribology study of pulse electrodeposited Ni-B-SWCNT composite coating, J. Occup. Med. 74 (2022) 574–583.
[20] F. Doğan, M. Uysal, E. Duru, H. Akbulut, S. Aslan, Pulsed electrodeposition of Ni-B/TiN composites: effect of current density on the structure, mechanical, tribological, and corrosion properties, J. Asian Ceram. Soc. 8 (4) (2020) 1271–1284.
[21] U.S. Waware, A.M.S. Hamoudaa, N.P. Wasekar, Mechanical properties, thermal stability and corrosion behavior of electrodeposited Ni-B/AlN nanocomposite coating, Surf. Coating. Technol. 337 (2018) 335–341.
[22] G. Yasin, M.A. Khan, M. Arif, M. Shakeel, T.M. Hassan, W.Q. Khan, R.M. Korai, Z. Abbas, Y. Zuo, Synthesis of spheres-like Ni/graphene nanocomposite as an efficient anti-corrosive coating; effect of graphene content on its morphology and mechanical properties, J. Alloys Compd. 755 (2018) 79–88.
[23] M. Tabish, M.U. Malik, M.A. Khan, G. Yasin, H.M. Asif, M.J. Anjum, W.Q. Khan, S. Ibraheem, T.A. Nguyen, Y. Slimani, M.T. Nazir, Construction of NiCo/graphene nanocomposite coating with bulges-like morphology for enhanced mechanical properties and corrosion resistance performance, J. Alloys Compd. 867 (2021), 159138.
[24] G. Yasin, M.J. Anjum, M.U. Malik, M.A. Khan, W.Q. Khan, M. Arif, T. Mehtab, T. A. Nguyen, Y. Slimani, M. Tabish, D. Ali, Y. Zuo, Revealing the erosion-corrosion performance of sphere-shaped morphology of nickel matrix nanocomposite strengthened with reduced graphene oxide nanoplatelets, Diam. Relat. Mater. 104 (2020), 107763.
[25] M.U. Malik, M. Tabish, G. Yasin, M.J. Anjum, S. Jameel, Y. Tang, X. Zhang, S. Manzoor, S. Ibraheem, W.Q. Khan, Electroless codeposition of GO incorporated silane nanocomposite coating onto AZ91 Mg alloy: effect of GO content on its morphology, mechanical and corrosion protection properties, J. Alloys Compd. 883 (2021), 160790.
[26] U. Pandey, R. Purohit, P. Agarwal, S.K. Dhakad, R.S. Rana, Effect of TiC particles on the mechanical properties of aluminium alloy metal matrix composites (MMCs), Mater. Today: Proc. 4 (2017) 5452–5460.
[27] B. Li, W. Zhang, T. Mei, Y. Miao, Fabrication of Ni-B/TiC-Y_2O_3 nanocomposites by one-step electrodeposition at different duty cycle and evaluation of structural, surface and performance as protective coating, J. Alloys Compd. 823 (2020), 153888.
[28] S. Dilek, H. Algül, A. Akyol, A. Alp, H. Akbulut, M. Uysal, Pulse electro co-deposition of submicron-sized TiC reinforced Ni–W coatings: tribological and corrosion properties, J. Asian Ceram. Soc. 9 (2) (2021) 673–685.
[29] B. Li, W. Zhang, Facile synthesis and electrochemical properties of a novel Ni-B/TiC composite coating via ultrasonic-assisted electrodeposition, Ultrason. Sonochem. 61 (2020), 104837.
[30] O. Fayyaz, A. Khan, R.A. Shakoor, et al., Enhancement of mechanical and corrosion resistance properties of electrodeposited Ni–P–TiC composite coatings, Sci. Rep. 11 (2021) 5327.
[31] S. Kaner, The Effect of aging treatments after TIG welding on AISI 304 stainless steel material on hardness and strength values, J. Politech. 24 (4) (2021) 1491–1498.
[32] H.H. Sheu, Y.C. Tzeng, J.H. Syu, Study of the strengthening mechanism of electrodeposited Ni-B thin films with ultra-low boron content, Mater. Lett. 238 (2019) 275–277.
[33] K. Belhamel, H. Kheraz, R. Ludwig, T.K.D. Nguen, N. Allsop, S.S. Al-Juaid, Electrodeposition and morphology analysis of nickel nanoparticles from sulphate bath, e-J. Surf. Sci. Nanotechnol. 8 (2010) 227–232.
[34] F. Doğan, Wear and Corrosion Behaviors of Ni-B-TiN MMC's Produced with Pulse Co-electrodeposition, PhD thesis, Institute of science, Sakarya University, 2020.
[35] I. Boukhoubza, M. Khenfouch, M. Achehboune, B.M. Mothudi, I. Zorkani, A. Jorio, X-ray diffraction investigations of nanostructured ZnO coated with reduced graphene oxide, J. Phys. 1292 (2019), 012011.
[36] P. Bindu, S. Thomas, Estimation of lattice strain in ZnO nanoparticles: X-ray peak profile analysis, J. Theor. Appl. Phys. 8 (2014) 123–134.
[37] M. Saleem, L. Fang, H.B. Ruan, F. Wu, Q.L. Huang, C.L. Xu, C.Y. Kong, Effect of zinc acetate concentration on the structural and optical properties of ZnO thin films deposited by Sol-Gel method, Int. J. Phys. Sci. 7 (23) (2012) 2971–2979.
[38] V. Bilgin, S. Köse, F. Atay, I. Akyüz, The effect of substrate temperature on the structural and some physical properties of ultrasonically sprayed CdS films, Mater. Chem. Phys. 94 (2005) 103–108.
[39] Z.R. Khan, M. Zulfequar, M.S. Khan, Optical and structural properties of thermally evaporated cadmium sulphide thin films on silicon (100) wafers, Mater. Sci. Eng. B 174 (2010) 145–149.
[40] G.B. Williamson, R.C. Smallman, Dislocation densities in some annealed and cold-worked metals from measurements on the x-ray Debye-Scherrer spectrum, Philos. Mag. A 8 (1) (1956) 34–46.
[41] A.L. Patterson, The Scherrer formula for X-ray particle size determination, Physical Rewiev 56 (1939) 978–982.
[42] W. Gu, C. Liu, J. Tang, R. Liu, H. Yang, J. Hu, Improving zinc electrodeposition in ammoniacal electrolytes with the saturated dissolved methyltrioctylammonium chloride, Hydrometallurgy 175 (2018) 43–51.

[43] A. Yousif, V. Kumar, R.M. Jafer, H.C. Swart, The effect of different annealing temperatures on the structure and luminescence properties of Y_2O_3:Bi^{3+} thin film fabricated by RF magnetron sputtering, Appl. Surf. Sci. 424 (3) (2017) 407–411.
[44] E. Ünal, A. Yaşar, İ.H. Karahan, A review of electrodeposited composite coatings with Ni-B alloy matrix, Mater. Res. Express 6 (2019), 092004.
[45] K. Shahzad, A.B. Radwan, O. Fayyaz, R.A. Shakoor, M. Uzma, M.A. Umer, M. N. Baig, A. Raza, Effect of concentration of TiC on the properties of pulse electrodeposited Ni-P-TiC nanocomposite coatings, Ceram. Int. 47 (13) (2021) 19123–19133.
[46] M. Alizadeh, A. Cheshmpish, Electrodeposition of Ni-Mo/Al_2O_3 nano-composite coatings at various deposition current densities, Appl. Surf. Sci. 466 (2019) 433–440.
[47] X. Shi, Z. Zhang, L. Dai, Y. Lv, Z. Xu, Y. Yin, Z. Liao, G. Wei, Effect of Al_2O_3 nanoparticles and heat treatment on the wear resistance of electrodeposited Ni-W/Al_2O_3 composite coatings, J. Mater. Eng. Perform. 31 (2022) 3094–3106.
[48] R.A. Shakoor, R. Kahraman, U.S. Waware, Y. Wang, W. Gao, Synthesis and properties of electrodeposited Ni–B–CeO_2 composite coatings, Mater. Des. 59 (2014) 421–429.
[49] H. Ogihara, M. Safuan, T. Saji, Effect of electrodeposition conditions on hardness of Ni–B/diamond composite films, Surf. Coating. Technol. 212 (2012) 180–184.
[50] N. Guglielmi, Kinetics of the deposition of inert particles from electrolytic baths, J. Electrochem. Soc. 119 (8) (1972) 1009–1012.
[51] V.S. Protsenko, F.I. Danilov, Kinetic model of composite coatings electrodeposition assuming irreversible adsorption of dispersed particles on a growing metal substrate, J. Electroanal. Chem. 918 (2022), 116463.
[52] M. Onado, K. Shimizu, Y. Tateishi, Mechanism of boron codeposition in electrodeposited Ni-B alloy films and calculation of the amount of codeposited boron, Trans. IMF 77 (1) (1999) 44–48.
[53] R. Oriňáková, K. Rošáková, A. Oriňák, M. Kupková, J.N. Audinot, H.N. Migeon, J. T. Andersson, K. Koval, Electrodeposition of composite Ni–B coatings in a stirred heterogeneous system, J. Solid State Electrochem. 15 (2011) 1159–1168.
[54] E. Ünal, İ.H. Karahan, Production and characterization of electrodeposited Ni-B/hBN composite coatings, Surf. Coating. Technol. 333 (2018) 125–137.
[55] E. Ünal, İ.H. Karahan, Investigation of effect of the bath components on coating properties in electrodeposition of Ni, Ni-B and Ni-B/hBN coatings, Sakarya Univ. J. Sci. 22 (2) (2018) 663–672.
[56] E. Ünal, İ.H. Karahan, Effects of ultrasonic agitation prior to deposition and additives in the bath on electrodeposited Ni-B/hBN composite coatings, J. Alloys Compd. 763 (2018) 329–341.
[57] R.A. Shakoor, R. Kahraman, U.S. Waware, Y. Wang, W. Gao, Properties of electrodeposited Ni-B-ZrO_2 composite coatings, Int. J. Electrochem. Sci. 10 (2015) 2110–2119.
[58] R.A. Shakoor, R. Kahraman, U.S. Waware, Y. Wang, W. Gao, Properties of electrodeposited Ni-B-Al_2O_3 composite coatings, Mater. Des. 64 (2014) 127–135.
[59] H. Ogihara, H. Wang, T. Saji, Electrodeposition of Ni–B/SiC composite films with high hardness and wear resistance, Appl. Surf. Sci. 296 (2014) 108–113.
[60] B. Li, W. Zhang, Y. Huan, J. Dong, Synthesis and characterization of Ni-B/Al_2O_3 nanocomposite coating by electrodeposition using trimethylamine borane as boron precursor, Surf. Coating. Technol. 337 (2018) 186–197.
[61] İ.H. Karahan, A. Aminifazl, T.D. Golden, Effect of TMAB concentration on structural, mechanical and corrosion properties of electrodeposited Ni–B alloys, J. Indian Chem. Soc. 99 (6) (2022), 100467.
[62] I. Manika, J. Maniks, Effect of substrate hardness and film structure on indentation depth criteria for film hardness testing, J. Phys. Appl. Phys. 41 (2008), 074010.
[63] F. Muktepavela, I. Manika, L. Grigorjeva, V. Skvortsova, Micromechanical properties of AlN, TiN, and AlN/TiN nanostructured multilayer coatings, in: Proc. SPIE 5122, Advanced Organic and Inorganic Optical Materials, 2003, https://doi.org/10.1117/12.515693.
[64] D.H. Kim, P. Hwang, J.K. Kim, M.L. Sham, Indentation properties of copper leadframe with hard coatings, Met. Mater. 4 (1998) 812–817.
[65] I. Manika, J. Maniks, Characteristics of deformation localization and limits to the microhardness testing of amorphous and polycrystalline coatings, Thin Solid Films 208/2 (1992) 223–227.
[66] J.H. Choi, G. Gyawali, D.R. Dhakal, J. Bhupendra, S.W. Lee, Electrodeposited Ni–W–TiC composite coatings: effect of TiC reinforcement on microstructural and tribological properties, Acta Metall. Sin. 33 (2020) 573–582.
[67] M. Ma, W. Sun, Y. Zhang, X. Liu, Y. Dong, J. Zi, Y. Xiao, Effect of TiC particles concentration on microstructure and properties of Ni-TiC composite coatings, Mater. Res. 22/6 (2019), e20190530.
[68] E. Danaila, L. Benea, N. Caron, O. Raquet, Titanium carbide nanoparticles reinforcing nickel matrix for improving nanohardness and fretting wear properties in wet conditions, Met. Mater. Int. 22 (2016) 924–934.
[69] M. Ganji, H. Yousefnia, Z.S. Seyedraoufi, Y. Shajari, The corrosion behavior of Ni-Fe and Ni-Fe-TiC nanoparticles deposited using pulse electrodeposition on low-carbon steel, J. Austral. Ceram. Soc. (2022), https://doi.org/10.1007/s41779-022-00747-w.
[70] E. Ünal, A. Yaşar, İ.H. Karahan, Investigation of the properties of Ni–B/TiC nanocomposite coatings produced at different particle concentrations by electrodeposition, Metall. Mater. Trans. 54 (2023) 2340–2361.
[71] O.R. Monteiro, S. Murugesan, V. Khabashesku, Electroplated Ni-B films and Ni-B metal matrix diamond nanocomposite coatings, Surf. Coating. Technol. 272 (2015) 291–297.
[72] M. Lekka, R. Offoiach, A. Lanzutti, M.Z. Mughal, M. Sebastiani, E. Bemporad, L. Fedrizzi, Ni-B electrodeposits with low B content: effect of DMAB concentration on the internal stresses and the electrochemical behaviour, Surf. Coating. Technol. 344 (2018) 190–196.
[73] S.M.A. Mousavi, R. Pitchumani, A study of corrosion on electrodeposited superhydrophobic copper surfaces, Corrosion Sci. 186 (2021), 109420.
[74] A.H.N. Nezhad, E.M. Zahrani, A.M. Alfantazi, Erosion-corrosion of electrodeposited superhydrophobic Ni-Al_2O_3 nanocomposite coatings under jet saline-sand slurry impingement, Corrosion Sci. 197 (2022), 110095.
[75] S. Kasturibai, G.P. Kalaignan, Characterizations of electrodeposited Ni–CeO_2 nanocomposite coatings, Mater. Chem. Phys. 147 (2014) 1042–1048.
[76] Y. Wang, S. Wang, X. Shu, W. Gao, W. Lu, B. Yan, Preparation and property of sol-enhanced Ni-B-TiO_2 nano-composite coatings, J. Alloys Compd. 617 (2014) 472–478.